

VUV-synchrotron absorption studies of N₂ and CO at 900 K

M. L. Niu^a, A. N. Heays^b, S. Jones^{b,c}, E. J. Salumbides^{a,d}, E. F. van Dishoeck^b,
N. De Oliveira^e, L. Nahon^e, W. Ubachs^{a,*}

^a*Department of Physics and Astronomy, LaserLaB, VU University, De Boelelaan 1081, 1081 HV Amsterdam, The Netherlands*

^b*Leiden Observatory, Leiden University, PO Box 9513, 2300 RA Leiden, The Netherlands*

^c*School of Physics and Astronomy, The University of Nottingham, University Park, Nottingham, NG7 2RD, United Kingdom*

^d*Department of Physics, University of San Carlos, Cebu City 6000, Philippines*

^e*Synchrotron Soleil, Orme des Merisiers, St. Aubin BP 48, 91192, Gif sur Yvette cedex, France*

Abstract

Photoabsorption spectra of N₂ and CO were recorded at 900 K, using the vacuum-ultraviolet Fourier-transform spectrometer at the DESIRS beamline of synchrotron SOLEIL. These high-temperature and high-resolution measurements allow for precise determination of line wavelengths, oscillator strengths, and predissociative line broadening of highly-excited rotational states with J up to about 50, and also vibrational hot bands. In CO, the perturbation of $A^1\Pi - X^1\Sigma^+$ vibrational bands (0,0) and (1,0) were studied, as well as the transitions to perturbing optically-forbidden states $e^3\Sigma^-$, $d^3\Delta$, $D^1\Delta$ and $a'^3\Sigma^+$. In N₂, we observed line shifts and broadening in several $b^1\Pi_u - X^1\Sigma_g^+$ bands due to unobserved forbidden states of $^3\Pi_u$ symmetry. The observed state interactions are deperturbed and, for N₂, used to validate a coupled-channels model of the interacting electronic states. This data is appropriate for use in astrophysical or (exo-)planetary atmospheric applications where high temperatures are important and in future spectroscopic models of these molecules.

Keywords: Synchrotron radiation, Fourier-transform spectroscopy, Carbon monoxide, Molecular nitrogen

1. Introduction

The technique of Fourier-transform spectroscopy is typically applied to the infrared and optical wavelength domains. The interferometric principle requires a beam-splitter for which no materials exist in the far vacuum ultraviolet (VUV) part of the electromagnetic spectrum. At the DESIRS beamline of the SOLEIL synchrotron [1] this problem was solved by developing a VUV Fourier-transform spectrometer (FTS) based on beam-splitting by wave-front division, thus enabling high-resolution spectroscopy at

wavelengths in the range 40 – 200 nm [2, 3]. In recent years, this unique instrument has been used to perform high resolution spectroscopic studies on a number of small molecules in the gas phase that exhibit strongly-structured multi-line spectra, such as H₂ [4], HD [5], N₂ [6], and CO [7]; as well as for molecules with more continuum-like spectra, such as CO₂ [8]. These studies amply demonstrate the multiplex advantage of the Fourier-transform technique by revealing many hundreds of absorption lines in a single-scan window of some 5 nm, determined by the bandwidth of the beam line undulator source. Alternatively, the setup was used to determine photo-absorption cross sections [9] and predissociation linewidths (and hence rates) of excited states of small molecules [6, 10].

*Corresponding author

Email address: w.m.g.ubachs@vu.nl (W. Ubachs)

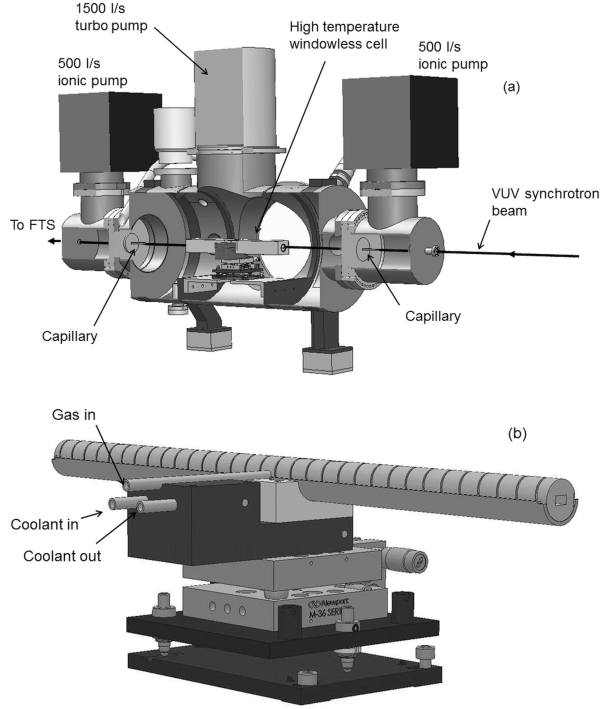


Figure 1: (a) Cross-section drawing of the gas sample chamber mounted in the FTS-branch of the DESIRS beam line at SOLEIL. The high temperature windowless cell is located in the center of the chamber and is separated from the ultra-high vacuum of the beamline by two stages of differential pumping. (b) The inset shows details of the cell and the shielding where half of the cylindrical shell has been removed for clarity. The heating element is wrapped all over the cylindrical cell inside a groove in order to increase surface contact with the cell. The gas is flowing through a 7.5×4.5 mm tube into the heated cell. The copper base can be cooled down with a thermalized water circulation system.

The FTS-VUV setup has been used for gas-phase absorption spectroscopy under varied measurement conditions. Most studies have been performed in a quasi-static gas environment where the gas sample effusively flows through a narrow capillary-shaped absorption cell, with the absorption path aligned with the VUV beam emanating from the undulator. This cell was not equipped with windows, to permit passage of the VUV beam through the sample gas into the FTS-VUV instrument for spectroscopic analysis. For this geometry, differential pumping maintains an ultrahigh vacuum in the FTS and DESIRS beam line. The column density of absorbing gas is limited by the pumping conditions and vacuum requirements of the beam line. In any case, there is a pressure gradient over the cell length falling off toward both ends, complicating any absolute column density calibration. In further studies dedicated to cross-section measurements, a movable gas cell was used of ~ 19 mm length and sealed by either MgF_2 or LiF wedged windows. This allowed for somewhat-higher pressures and controlled gas column densities [11]. Studies using this cell are limited in wavelength range to $\lambda > 105$ nm [12] by the short-wavelength opacity of the windows. In some experiments requiring the simplification of congested spectra, a molecular jet expansion was employed as well as cooling of the quasi-static gas cell with liquid-nitrogen or liquid-helium. A comparison between these techniques was performed in a study of the D_2 spectrum [13] which also demonstrated improved spectral resolution and accuracy through reduction of the Doppler width under these conditions.

For the present study a heated cell is implemented, allowing for the recording of spectra at temperatures of ~ 1000 K. The high-resolution FTS allows for the measurement and analysis of severely congested spectra at these elevated temperatures. Such spectra bear significance for the modeling of astrophysical shock-wave regions [14], or other high-temperature astrophysical regions where the spectroscopy of small molecules is key to understanding the phenomena, such as e.g., in the photospheres of white dwarfs [15]. Another goal of performing spectroscopy of hot samples is to follow rotational progressions to high J -quantum numbers, where perturbations due to non-

Born-Oppenheimer effects are abundantly present. Some pertinent perturbation features specifically occurring at high rotational quantum numbers will be shown here in VUV-absorption spectra of CO and N₂ recorded at 900 K.

2. Experimental

The VUV Fourier-Transform spectrometer at the DESIRS beamline is a permanent end station dedicated to high-resolution photoabsorption studies in the range 4 – 30 eV [1]. The instrument has been described in detail previously [2, 3]. In short, the spectrometer is based on wave-front division interferometry using reflective surfaces, thus allowing the extension of the FTS technique into the far VUV spectral range. The undulator white beam is used as the background, feeding the FTS branch and permits the recording of a spectral bandwidth $\Delta E/E = 7\%$, corresponding to 5 nm, on each scan. The typical integration time for a single scan is less than 30 minutes to obtain a signal-to-noise ratio for the background continuum level of ~ 400 .

The windowless absorption cell is a 40 cm long T-shaped tube with a rectangular cross section, installed under vacuum inside the multi-purpose gas sample chamber of the FTS branch (Fig. 1). The cross section of the tube (7.5×4.5 mm) is adapted to the astigmatic shape and dimensions of the undulator source in this section of the beam line. An Inconel heating element (thermocox) is wrapped around the tube sitting in a groove designed to maximize the contact surface between the heating wire and the cell, and ensuring the gas flowing in the tube is uniformly heated. Two semi-cylindrical shells are pressed around the cell in order to improve the thermal contact during the heating operation. An extra stainless steel box is also installed to shield radiation originating from the cell. Inconel allows for heating the cell up to 1000 K, although, the present measurements were done at a maximum temperature of 900 K. The cell is mounted on a copper base plate that can be cooled by water circulation, although during the experiments the setup was operated without the cooling system. The temperature of the base-mount was carefully monitored within the covered range of

temperature (for the cell) and never went beyond a maximum of 200°C with no visible consequence or damage. A thermocouple is connected at one end of the cell to obtain an indication of the gas temperature. The quasi-static gas density inside the heated cell was monitored from outside the vacuum by a 1 mbar range capacitive gauge. The gas column density was adjusted by a needle valve in order to have a constant continuous flow through the cell during the photoabsorption measurements. The effective column density along the absorption path inside the cell varied from 4×10^{14} to 1.2×10^{17} cm⁻² and was adjusted according to the cross sections of the recorded bands.

In the present study, the FTS-VUV was set to provide an instrumental linewidth of 0.27 cm⁻¹. The Doppler broadening corresponds to 0.28 cm⁻¹ at a frequency of 65 000 cm⁻¹, temperature of 900 K, and molecular mass of 28 amu. After convolution with the instrument width, a spectral linewidth of 0.39 cm⁻¹ is anticipated for unsaturated and non-predissociation-broadened N₂ and CO lines. The FTS spectra are intrinsically wavelength calibrated by monitoring the movement of the travel arm in the interferometer which is controlled by a HeNe-laser [2, 3]. Additional and improved calibration can be derived from co-recording special calibration lines, e.g. resonance lines of noble gases [16, 17]. In the present case of the CO spectra the very accurate laser-calibration data of the low-*J* rotational lines in the *A* – *X* bands, accurate to $\Delta\lambda/\lambda = 3 \times 10^{-8}$, were used [18]. For the present high-temperature measurements with larger Doppler-broadening the FTS was not used in its very highest resolution mode and the spectral accuracy typically reached is estimated at 0.02 cm⁻¹. The accuracy is somewhat lower for weaker and blended lines.

3. Absorption spectra of N₂

Five N₂ vibrational bands were analysed appearing in our spectrum between 100 400 and 108 500 cm⁻¹ (99.6 and 92.2 nm). These bands are spectroscopically denoted $b^1\Pi_u - X^1\Sigma_g^+(v', v'' = 0)$ for $v' = 0, 1, 2$, and 10, and $c'_4^1\Sigma_u^+ - X^1\Sigma_g^+(v' = 0, v'' = 1)$

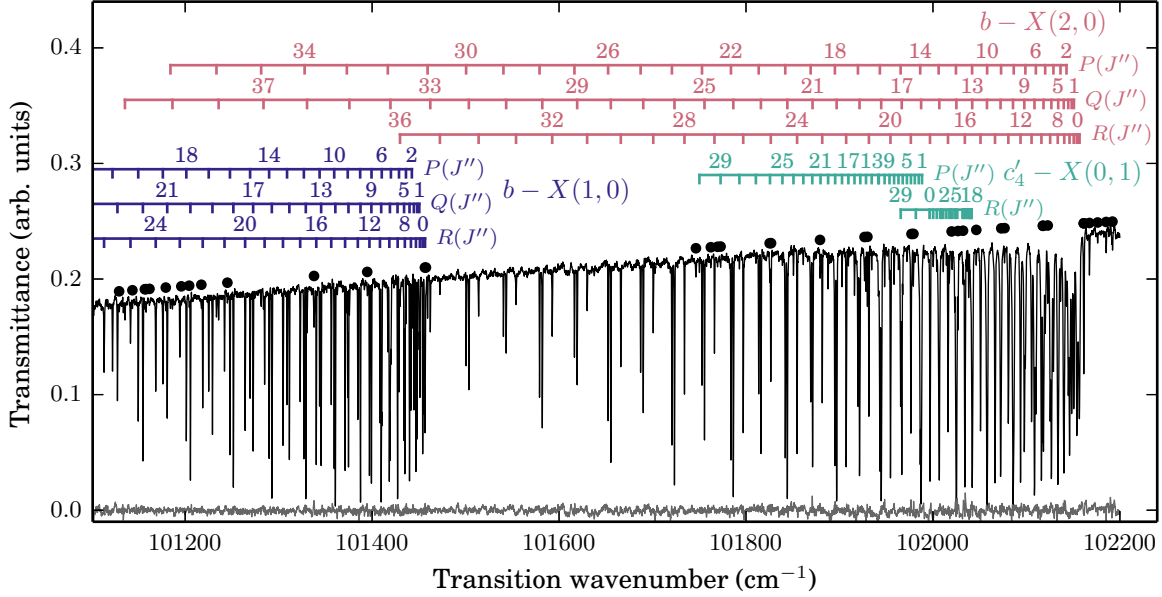


Figure 2: Photoabsorption spectrum showing the bands $b-X(2,0)$, $c'_4-X(0,1)$, and part of $b-X(1,0)$; and further absorption lines arising from H_2 contamination, high- J' lines of $b-X(3,0)$, and of unknown origin (*circles*). The lower trace indicates the residual error after subtracting a model spectrum.

(where v' and v'' are upper- and lower-state vibrational quantum numbers, respectively; and hereafter we neglect electronic-state term symbols); and have been previously observed in room-temperature or expansion-cooled synchrotron- or laser-based experiments [19, 20, 21, 22, 23, 24]. Part of our photoabsorption spectrum showing three of these bands is plotted in Fig. 2. A listing of the deduced term values for the e and f components of the observed $b(v')$ levels is given in Table 1.

The analysis of DESIRS FTS spectra of molecular nitrogen has been discussed previously [6]. This involves simulating each observed absorption line with a Voigt profile defined by a Gaussian Doppler width, Lorentzian natural line width, transition wavenumber, and integrated cross section. A summed cross section is then transformed into an absorption spectrum by the Beer-Lambert law and convolved with a sinc function simulating the instrumental resolution of the FTS. All parameters defining the model absorption spectrum are then automatically optimised to best agree with the experimental scan.

In many cases a more useful measurement of the strength of a line than the integrated cross section is a derived band f -value, calculated by factoring the ground-state rotational thermal population as well as rotation-dependent Hönl-London linestrength factors. Band f -values are only weakly dependent on upper-state J' for unperturbed bands.

The main difficulties encountered while analysing the hot-cell N_2 spectrum were the significant contamination from highly-excited rotational structure of nearby bands and obtaining a correct calibration of the temperature in the cell. Groups of lines from the same vibrational band were sometimes analysed while assuming correlated wavenumbers, widths and strengths to facilitate the analysis of blended spectral regions. That is, $P(J''-1)$ and $R(J''+1)$ transitions are connected to a common excited state so the difference in their transition wavenumbers was fixed to known ground-state energy levels [34] and a common linewidth assumed. A weak J' -dependence (or J' -independence) was also assumed for some linewidths or f -values.

Table 1: Experimental upper term values^a for observed lines in N₂ indexed by excited state angular-momentum, J' .

J'	$b(0)$		$b(1)$		$b(2)$		$b(10)$
	e -parity	f -parity	e -parity	f -parity	e -parity	f -parity	e/f -parity ^b
1	100 819.84(2)	100 819.91(4)	101 454.460(5)	101 454.455(8)	102 154.82(1)	102 154.79(3)	108 374.115(7)
2	100 825.54(3)	100 825.61(1)	101 460.090(7)	101 460.097(3)	102 160.33(1)	102 160.359(7)	108 378.968(4)
3	100 834.25(1)	100 834.27(2)	101 468.560(2)	101 468.541(4)	102 168.691(5)	102 168.658(9)	108 386.239(4)
4	100 845.85(2)	100 845.821(9)	101 479.798(4)	101 479.803(3)	102 179.754(8)	102 179.731(8)	108 395.955(4)
5	100 860.303(7)	100 860.32(1)	101 493.874(2)	101 493.877(3)	102 193.637(4)	102 193.70(1)	108 408.050(2)
6	100 877.67(1)	100 877.660(8)	101 510.764(3)	101 510.75(1)	102 210.295(7)	102 210.267(6)	108 422.591(3)
7	100 897.887(6)	100 897.895(9)	101 530.443(2)	101 530.456(4)	102 229.655(4)	102 229.675(8)	108 439.530(2)
8	100 921.01(1)	100 920.987(7)	101 552.946(2)	101 552.940(3)	102 251.874(9)	102 251.846(8)	108 458.875(2)
9	100 946.968(6)	100 946.96(1)	101 578.238(2)	101 578.24(1)	102 276.746(6)	102 276.770(9)	108 480.618(2)
10	100 975.83(1)	100 975.815(7)	101 606.338(3)	101 606.348(6)	102 304.416(6)	102 304.426(7)	108 504.758(2)
11	101 007.503(6)	101 007.52(3)	101 637.230(2)	101 637.230(3)	102 334.845(3)	102 334.856(7)	108 531.283(2)
12	101 042.036(9)	101 042.04(1)	101 670.911(2)	101 670.912(3)	102 368.018(4)	102 368.018(7)	108 560.191(2)
13	101 079.458(7)	101 079.44(1)	101 707.379(2)	101 707.378(3)	102 403.933(3)	102 403.926(8)	108 591.479(2)
14	101 119.70(1)	101 119.690(8)	101 746.629(2)	101 746.626(3)	102 442.572(3)	102 442.635(8)	108 625.157(2)
15	101 162.74(1)	101 162.74(1)	101 788.652(2)	101 788.654(3)	102 483.948(2)	102 483.965(6)	108 661.209(2)
16	101 208.58(2)	101 208.600(9)	101 833.455(2)	101 833.456(3)	102 528.044(3)	102 528.086(5)	108 699.644(2)
17	101 257.250(9)	101 257.29(2)	101 881.006(2)	101 881.013(3)	102 574.875(2)	102 574.887(4)	108 740.459(3)
18	101 308.77(2)	101 308.71(1)	101 931.329(3)	101 931.332(3)	102 624.387(3)	102 624.415(4)	108 783.684(5)
19	101 362.95(1)	101 362.91(3)	101 984.400(2)	101 984.400(4)	102 676.610(2)	102 676.647(4)	108 829.02(1) ^c
20	101 419.98(3)	101 419.92(1)	102 040.210(3)	102 040.215(3)	102 731.545(3)	102 731.574(3)	108 876.398(7)
21	101 479.69(2)	101 479.66(4)	102 098.767(2)	102 098.764(5)	102 789.153(2)	102 789.168(4)	108 926.565(6)
22	101 542.27(6)	101 542.13(3)	102 160.044(4)	102 160.042(3)	102 849.447(2)	102 849.489(3)	108 979.148(5)
23	101 607.38(2)	101 607.27(6)	102 224.043(3)	102 224.045(6)	102 912.413(2)	102 912.457(4)	109 034.005(5)
24	—	101 675.24(3)	102 290.766(6)	102 290.761(4)	102 978.050(3)	102 978.097(3)	109 091.321(4)
25	101 745.90(5)	101 745.66(7)	102 360.177(4)	102 360.171(8)	103 046.349(2)	103 046.384(4)	109 150.906(5)
26	—	101 819.01(6)	102 432.300(8)	102 432.275(6)	103 117.309(4)	103 117.327(3)	109 212.899(4)
27	101 895.03(5)	—	102 507.081(5)	102 507.08(1)	103 190.873(2)	103 190.911(5)	109 277.088(7)
28	—	101 973.59(9)	102 584.52(1)	102 584.532(8)	103 267.083(4)	103 267.124(4)	109 343.734(9)
29	—	—	102 664.686(8)	102 664.67(2)	103 345.914(3)	103 345.956(6)	109 412.79(1)
30	—	102 138.44(6)	102 747.45(4)	102 747.45(1)	103 427.360(6)	103 427.403(5)	109 484.23(4)
31	—	—	102 832.91(1)	102 832.83(3)	103 511.408(4)	103 511.446(8)	—
32	—	—	—	102 920.94(2)	103 598.05(1)	103 598.083(6)	—
33	—	—	103 011.62(3)	—	103 687.265(6)	103 687.32(1)	—
34	—	—	—	—	103 779.06(1)	103 779.09(2)	—
35	—	—	—	—	103 873.41(1)	103 873.46(2)	—
36	—	—	—	103 299.14(5)	103 970.27(3)	103 970.33(2)	—
37	—	—	—	—	104 069.79(4)	104 069.80(5)	—
38	—	—	—	—	—	104 171.73(4)	—
39	—	—	—	—	—	104 276.17(9)	—
40	—	—	—	—	—	104 383.05(5)	—

^aWith units of cm⁻¹ and parenthetical 1 σ fitting uncertainties in terms of the least-significant digit. The estimated absolute calibration uncertainty is 0.04 cm⁻¹.

^bNo splitting of e - and f - parity levels was observed (apart from for $J' = 18$) and these were assumed identical.

^cA splitting of e - and f - parity levels was observed, with term values 108 829.02(1) and 108 828.82(3) cm⁻¹, respectively.

Lines with natural widths below about 0.05 cm^{-1} full-width half-maximum (FWHM) are not reliably measured in our experiment due to concurrent instrument and Doppler broadening by 0.27 and about 0.4 cm^{-1} FWHM, respectively. No linewidths are then measurable from our spectrum for transitions to the weakly-predissociated $c'_4(0)$ level [25].

We compare our measured f -values and linewidths with those calculated from an existing model of N_2 photoabsorption and dissociation, including photoabsorbing $^1\Pi_u$ and $^1\Sigma_u^+$ excited states and spin-forbidden but dissociative $^3\Pi_u$ states [6, 26, 27, 28, 29]. This model solves a coupled-Schrödinger equation (CSE) for the nuclear motion of the excited molecule, where the necessary potential-energy curves and state interactions have been optimised with respect to a large body of room-temperature experimental data. This model has been successfully employed previously in applications of atmospheric [30] and astronomical photochemistry [31, 32], including temperatures as high as 1000 K . Here, we seek to validate the extrapolation of the CSE model to high temperature by comparison to our new measurements.

3.1. Temperature calibration

The f -values of $b - X(v', 0)$ transitions were used to calibrate the ground-state rotational temperature and N_2 column density in the hot cell by comparison with previously-measured absolutely-calibrated f -values for $v' = 0, 1, 2$, and 10 [23, 24]. The resultant values are $(6.35 \pm 0.64) \times 10^{15}\text{ cm}^{-2}$ and $901 \pm 26\text{ K}$, respectively. The reference data was recorded at room temperature, included rotational levels as high as $J = 23$, and themselves have an absolute column density uncertainty of 10% which is also the dominant systematic uncertainty of our f -values. The final agreement between the present measurements and the reference data, shown in Fig. 3, is very good despite the factor-of-5 difference in ground state populations, for example, at $J' = 20$.

The $c'_4 - X(0, 1)$ band appears quite weakly in our spectrum and was analysed in order to estimate the vibrational temperature in the hot cell. For this, constant band f -values were assumed over

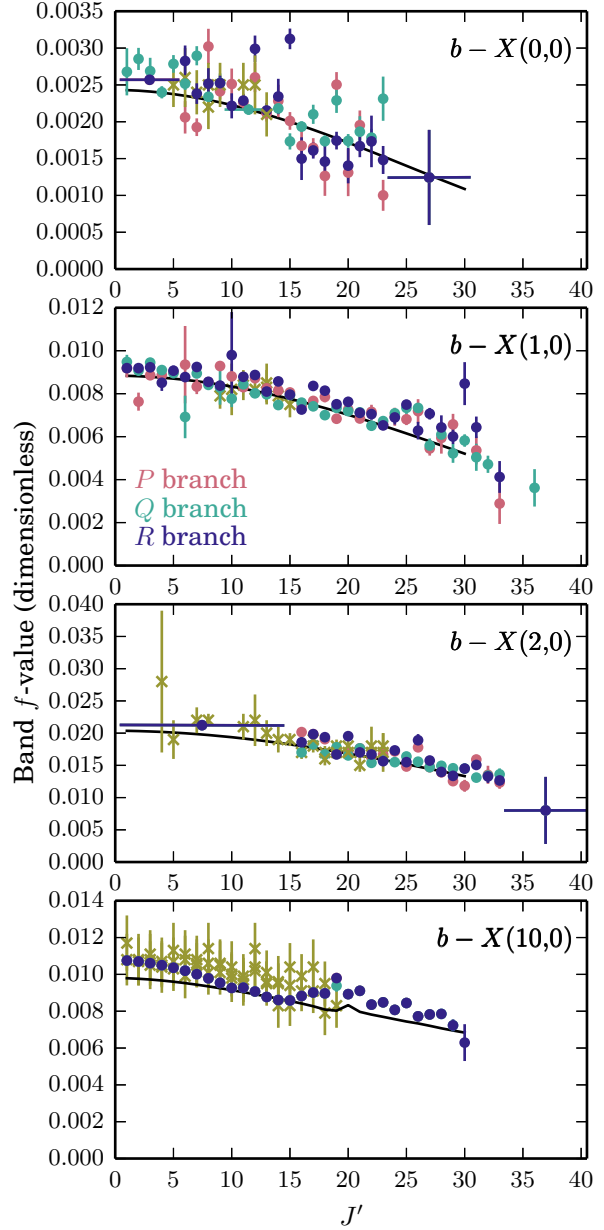


Figure 3: Band f -values of all transitions observed in our experiment as a function of excited-state angular-momentum quantum number, J' , and with 1σ random fitting uncertainties (circles with error bars). A 10% systematic error also applies and some f -values were analysed assuming J' -independent ranges (horizontal error bars). Also shown are previously-measured f -values [23, 24] (crosses), and calculated by the CSE model (solid black curves).

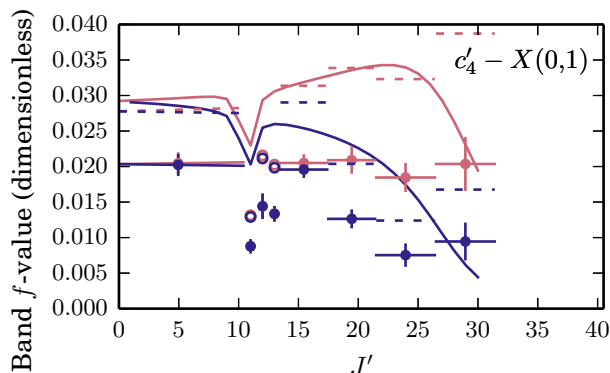


Figure 4: Band f -values of all $c'_4 - X(0,1)$ transitions observed in our experiment as a function of excited-state angular-momentum quantum number, J' , and with 1σ random fitting uncertainties (circles with error bars). A 10% systematic error also applies and some f -values were analysed assuming J' -independent ranges (horizontal error bars). Also shown are alternative experimental f -values assuming an 800 K ground state excitation (dashed lines, open circles) and reference values calculated from a combination of CSE and experimental data (solid curve).

small ranges of most $P(J'')$ and $R(J'')$ lines as indicated piecewise in Fig. 4. Simulated $c'_4 - X(0,1)$ f -values are also shown, with magnitude calculated from the ratio of $c'_4 - X(0,0)$ and $c'_4 - X(0,1)$ f -values deduced by electron-excited fluorescence [33], $f_{(0,0)}/f_{(0,1)} = 6.3 \pm 0.4$, and an absolute $c'_4 - X(0,0)$ absorption f -value measurement [23]. The stated uncertainties of the two experimental values used in this comparison are 6% [33] and 10% [23], respectively, although the latter should be neglected because our experimental column-density is calibrated to the same reference. We used the CSE model to simulate the significant rotational dependence of $c'_4 - X(0,1)$ f -values and assumed a 900 K distribution of ground-state rovibrational levels. This simulation then correctly reproduced the observed splitting of P - and R -branch f -values for $c'_4 - X(0,1)$ transitions with increasing J' . This splitting is also known to occur for the $c'_4 - X(0,0)$ fundamental band [23] and is the result of a rotational-perturbation of $c'_4(v' = 0)$ by nearby $^1\Pi_u$ levels [6]. Additionally, $c'_4 - X(0,1)$ transitions to $J' = 11, 12$, and 13 levels are significantly weakened relative to their neighbours due to

a well-known localised perturbation by the crossing rotational term series of $b'^1\Sigma_u^+(v' = 1)$ [20].

The newly-measured $c'_4 - X(0,1)$ f -values are somewhat smaller than the simulated values and an alternative model adopting an 800 K distribution of ground-state levels leads to the better agreement indicated in Fig. 4. This may indicate incomplete thermalisation of the N_2 in our experiment leading to a lesser degree of vibrational excitation than rotational. A similar result is found in Sec. 4 for the CO rotational and vibrational temperatures.

As a final check on the temperature of our sample of N_2 , the Doppler broadening in our experiment was measured by reference to lower- J' levels of the $b - X(1,0)$ absorption band, whose predissociation broadening is known to be below our resolution limit [21, 26]. We find a kinetic temperature from this of about 930 K, with an uncertainty estimated to be significantly greater than for our deduced rotational temperature.

3.2. Results

Transition wavenumbers for all observed $b - X(v', 0)$ bands were reduced to term values using accurate N_2 ground-state molecular constants [34]. Term values for these bands have been deduced previously for rotational levels with J' as high as 36 and with about 0.1 cm^{-1} uncertainty. Our term values are listed in Table 1 and have statistical uncertainties of around 0.01 cm^{-1} . The absolute calibration of our experiment was made by comparison of argon resonance lines appearing in our spectra with the NIST database and has an estimated uncertainty of 0.04 cm^{-1} .

Our deduced band f -values are plotted in Fig. 3. The decrease of $b - X(v', 0)$ f -value with J' continues to the highest-excitation lines that we observe and is in perfect agreement with values predicted by the CSE model. This decrease is effectively due to a decreasing Franck-Condon overlap of $b(v')$ and $X(0)$ vibrational wave functions with increasing centrifugal distortion.

Measured natural linewidths and comparable values from previous photoabsorption and resonantly-enhanced photoionisation experiments [19, 22, 23] are shown in Fig. 5. The widths of $b(0)$, $b(1)$, and $b(2)$

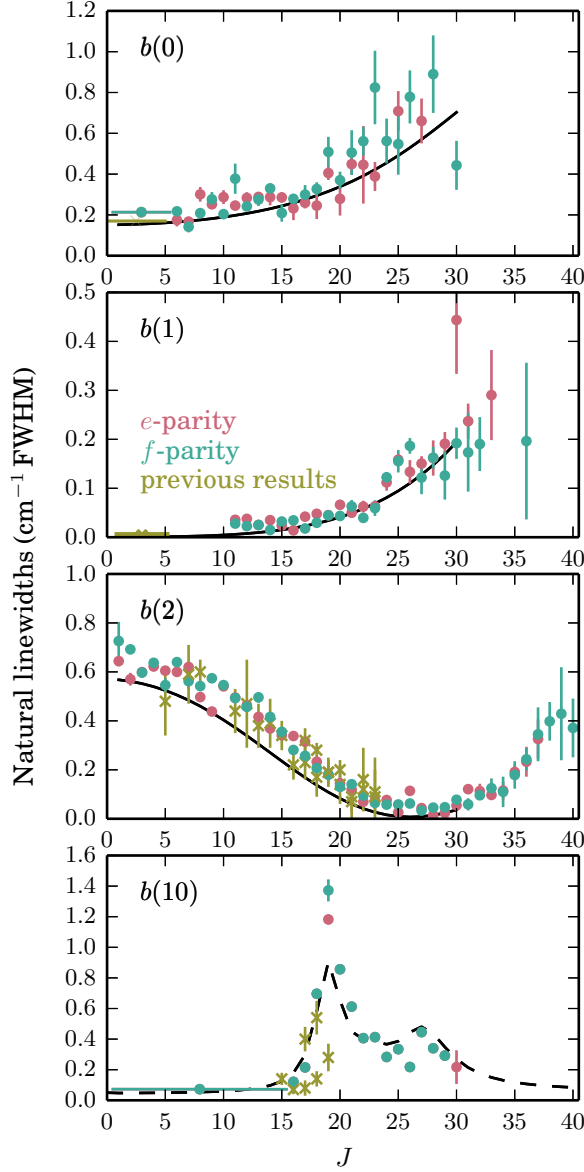


Figure 5: Natural linewidths of e - and f -parity excited-state levels accessed in our experiment as a function of their angular-momentum quantum number, J' , and with 1σ random fitting uncertainties (circles with error bars). Some linewidths were analysed assuming J' -independent ranges (horizontal error bars). Also shown are previously-measured linewidths [19, 21, 22, 23, 24] (yellow lines and crosses), and linewidths calculated by the CSE model (solid black curves) and a two-level local interaction model (dashed black curve).

averaged over their $J \leq 5$ levels have been previously deduced from laser-based lifetime or linewidth measurements [19, 21, 22]. The rotationally-resolved J -dependent broadening of $b(2)$ and $b(10)$ levels have been measured in synchrotron-based experiments [23, 24], and an increasing $b(1)$ predissociation width with J' has also been experimentally deduced [35, 36]. Our newly-measured widths show good agreement with all reference data but with generally reduced scatter. Two interesting new pieces of information are discussed below.

First, the decreasing $b(2)$ widths are now shown to pass through a minimum at $J \simeq 28$. This complex behaviour is well-reproduced by the CSE model which includes a mechanism for predissociative line broadening by including unbound electronic states amongst its coupled channels [26, 27]. The critical interactions in this case are the spin-orbit coupling of $b(2)$ with vibrationally-bound levels of the $C^3\Pi_u$ state and their subsequent electronic interaction with the unbound continuum of the $C'^3\Pi_u$ state. The dominant perturber of $b(2)$ is the $C(8)$ level which lies only 100 cm^{-1} lower in energy and has been previously identified in a photoabsorption spectrum [37] and found to have a linewidth of 18 cm^{-1} for J' less than about 10, despite the nominally spin-forbidden nature of this transition. All other bound $^3\Pi_u$ states are too remote in energy to contribute significantly to the predissociation of $b(2)$ [28] and the observed J' -dependence of its widths must then closely scale with the broader widths of $C(8)$.

Second, there is a sharp peak in the linewidths of $b(10)$ shown in Fig. 5. Increasing widths beginning around $J' = 15$ were known from a poorer signal-to-noise-ratio room-temperature spectrum [24], but are now better resolved and to higher- J' . There is also a perturbation of $b(10)$ rotational energy levels near $J' = 19$, as shown in Fig. 6 as a 0.8 cm^{-1} deflection of its reduced term values. The localised perturbation of $b(10)$ energies and widths indicates a level crossing with a predissociation-broadened level of $^3\Pi_u$ symmetry, as is known to occur elsewhere in the N_2 spectrum [37].

One candidate for the role of $b(10)$ perturber is the $v' = 16$ level of the $C^3\Pi_u$ state, which has been observed for $J' \leq 10$ [37] and has a band

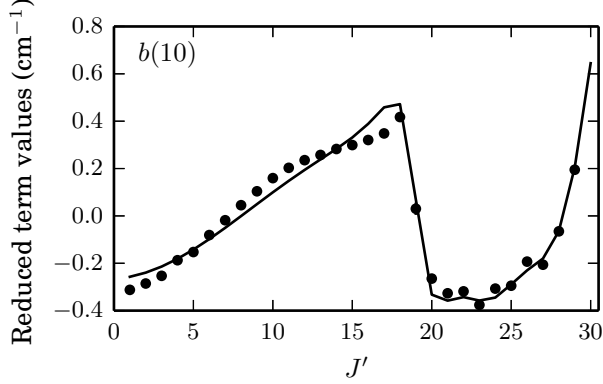


Figure 6: Experimental f -parity term values of $b(10)$ reduced by the subtraction of a cubic polynomial of best fit in terms of $J'(J' + 1)$ (circles). Also shown are reduced term values from the $b(10)/^3\Pi_u$ interaction model (curve).

origin only 80 cm^{-1} below that of $b(10)$. However, a rotational constant calculated from the observed $C(16)$ levels, 1.153 cm^{-1} [28], is too low to cross the $b(10)$ term series where the observed perturbation peaks at $J \simeq 18$. Alternatively, the $v = 2$ level of the $G^3\Pi_u$ state has been observed [38] to lie nearby, 340 cm^{-1} below $b(10)$, and undoubtedly has a larger rotational constant more characteristic of N_2 Rydberg levels, about 1.9 cm^{-1} . A crossing between $G(2)$ and $b(10)$ is then conceivable. The observed widths of $C(16)$ for $J' \leq 10$ are less than 0.5 cm^{-1} FWHM, whereas $G(2)$ is predicted to be much broader, about 90 cm^{-1} FWHM, by the CSE model of Lewis *et al.* [28].

To analyse the width and term value perturbation of $b(10)$ further we defined a two-level model of $b(10)$ interacting by the spin-orbit operator with a $^3\Pi_u$ level (including all triplet sublevels) and optimised its various parameters to match our experimental data. This was done in an identical fashion to similar deperturbations of N_2 $^3\Pi_u/1\Pi_u$ interactions by Lewis *et al.* [37]. Comparisons of experimental widths and reduced term values with this model are shown in Figs. 5 and 6 and find overall good agreement when adopting a $^3\Pi_u$ state with a term origin of approximately $108\,150\text{ cm}^{-1}$, a rotational constant of 1.6 cm^{-1} , and a spin-orbit splitting of 30 cm^{-1} (where the sign of the latter is unconstrained). Two further

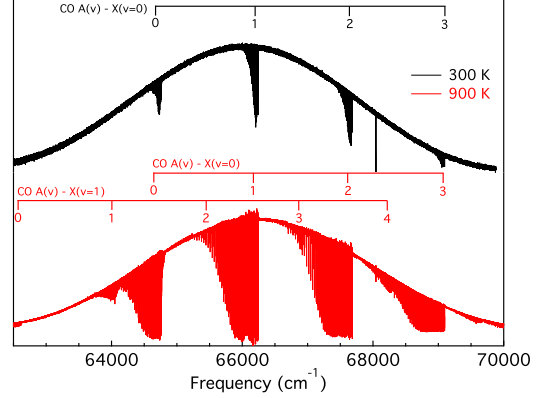


Figure 7: Overview spectrum of the $\text{CO } A^1\Pi - X^1\Sigma^+$ system including (0,0), (1,0), and (2,0) bands, and some hot bands. The top panel shows the spectrum which is measured at room temperature (300 K). In the bottom panel is the hot spectrum (900 K). The sharp absorption line in the upper spectrum at 68045.156 cm^{-1} is a xenon resonance line.

model parameters are the strength of the $b(10)$ and $^3\Pi_u$ spin-orbit interaction, 7 cm^{-1} , and the deperturbed predissociation widths of $^3\Pi_u$ levels. Good agreement could only be found when assuming the latter increases linearly in term of $J'(J' + 1)$ from 20 cm^{-1} at $J' = 18$, to 60 cm^{-1} at $J' = 29$. All of these deduced values are intermediate between those known or predicted for $C(16)$ and $G(2)$, [28, 37, 38], indicating that the perturber of $b(10)$ is an electronic admixture of the $C^3\Pi_u$ and $G^3\Pi_u$ states. Indeed, the coupled-channels model of Lewis *et al.* [28] predicts this, as well as a further significant admixture of the $F^3\Pi_u$ Rydberg state into the nominal $C(16)$ and $G(2)$ levels.

4. Absorption spectra of $\text{CO } A-X(0,0)$ and (1,0) bands

The novel hot cell configuration was employed for the further investigation of the $A^1\Pi - X^1\Sigma^+$ system of CO for the lowest vibrational bands in the excited state. Figure 7 shows an overview spectrum of some bands recorded at 300 K and 900 K. With the higher gas temperature, the rotational envelope of each band includes higher J -quantum numbers and hot bands

Table 2: Observed high- J transition frequencies (in vacuum cm^{-1}) of the CO $A^1\Pi - X^1\Sigma^+(0,0)$ and $(1,0)$ bands obtained with the hot cell. Lower- J transitions are listed in Ref. [7]. The estimated uncertainty (1σ) is 0.02 cm^{-1} except for weak or blended lines.

$A^1\Pi - X^1\Sigma^+(0,0)$				$A^1\Pi - X^1\Sigma^+(1,0)$			
J''	R(J)	Q(J)	P(J)	J''	R(J)	Q(J)	P(J)
17			64589.64	21	66140.33		66005.05
18			64583.37	22	66128.24		65986.78
19	64689.77		64566.32	23	66115.44		65967.83
20	64679.86		64549.58	24	66101.66	66023.95	65948.17
21	64669.38		64532.53	25	66091.32	66006.31	65927.76
22	64658.26	64584.85	64515.00	26	66074.03	65989.04	65906.37
23	64646.44	64570.02	64496.90	27	66058.34	65970.28	65888.43
24	64634.07	64554.44	64478.17	28	66042.09	65950.94	65863.57
25	64620.76	64538.20	64458.80	29	66025.18	65929.54	65840.31
26	64604.44	64521.15	64438.67	30	66007.60	65910.53	65816.49
27	64593.32	64501.07	64417.88	31	65989.33	65889.04	65792.02
28	64577.54	64486.13	64393.98	32	65970.28	65866.89	65766.89
29	64559.78	64466.58	64375.28	33	65950.64	65843.98	65741.06
30	64551.43	64445.05	64351.94	34	65930.24	65819.92	65714.55
31	64531.64	64432.91	64326.63	35	65909.14	65798.34	65687.33
32	64512.56	64409.35	64310.71	36	65887.33	65772.41	65659.43
33	64490.76	64386.49	64283.40	37	65864.79	65746.65	65630.83
34	64481.53	64360.95	64256.77	38	65841.53	65720.29	65601.52
35	64459.85	64347.94	64227.48	39	65817.50	65693.27	65571.51
36	64438.85	64322.50	64210.71	40	65793.18	65665.55	65540.79
37		64297.87	64181.54	41	65767.61	65637.11	65509.30
38	64396.16	64272.94	64153.19	42	65741.50	65607.95	65477.54
39	64373.87	64248.16	64124.55	43	65714.55	65577.99	65444.54
40	64350.93	64221.59	64095.36	44	65686.94	65548.84	65410.97
41	64327.65	64194.95	64065.55	45	65658.53	65516.48	65376.69
42	64303.14	64167.66	64035.39	46	65628.96	65484.32	65341.67
43	64278.62	64139.56	64004.55	47	65600.90	65451.21	65305.83
44	64253.03	64111.24	63972.67	48	65569.47	65418.96	65268.92
45	64226.85	64081.88	63940.64	49	65537.24	65383.97	
46	64199.92	64052.09	63907.71	50		65348.14	
47	64172.37			51		65318.08	
48		63989.48		52		65277.96	
51		63892.98		53	65402.39		

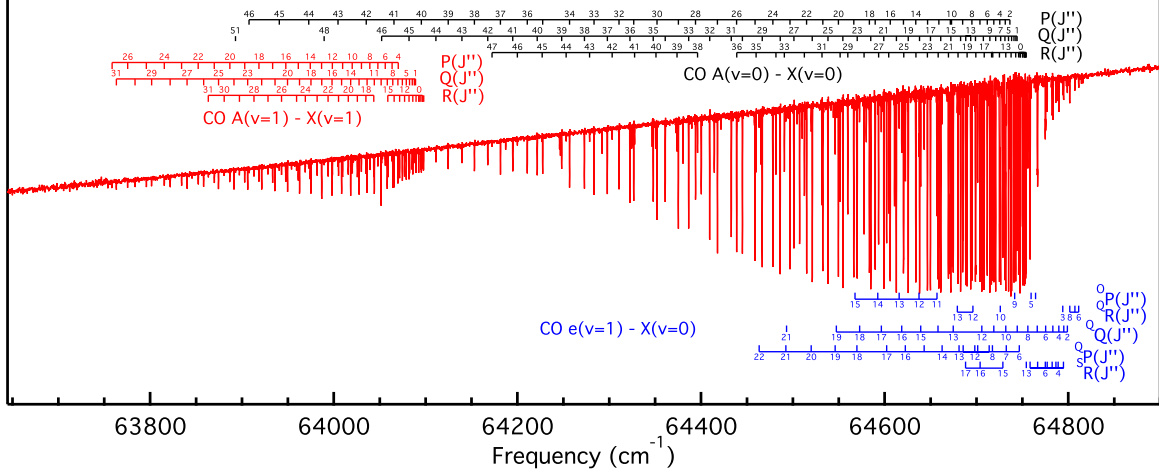


Figure 8: (*Preferably printed in two-column*) The spectrum of the CO $A^1\Pi - X^1\Sigma^+$ system in the range 63 700 – 64 900 cm^{-1} measured using the hot cell in combination with the FTS-VUV. Rotational lines in the $A - X$ (0,0) and (1,1) bands are assigned by the sticks. Transitions to the $e^3\Sigma^-$ perturber state are also assigned. The slope on the background continuum is due to the spectral profile of the undulator emission.

appear that originate from $X^1\Sigma^+(v'' = 1)$. Figure 8 displays a more detailed spectrum of the (0,0) and (1,1) bands of the $A^1\Pi - X^1\Sigma^+$ system of CO. Note that the strongest transitions in Figs. 7 and 8 are saturated. A number of spectra were recorded at various gas densities so that transition frequencies for all lines could be analysed in unsaturated recordings. The observed high- J transition frequencies in the $A^1\Pi - X^1\Sigma^+(0,0)$ and (1,0) bands are collected in Table 2. While in a previous room temperature study of the same bands their rotational progression could be followed up to $J = 21$ and $J = 23$, respectively [7], the present spectrum reveals lines up to $J = 51$ and $J = 53$ for the two bands. Accurate transition frequencies for low- J transitions were already given in Ref.[7].

In the observed region, between 63 500 – 67 500 cm^{-1} , many lines were observed that excite perturber states of the $A^1\Pi$ ($v = 0$) and ($v = 1$) levels, and are examined in the present study. Lines pertaining to the $e^3\Sigma^- - X^1\Sigma^+$ (1,0) band, clearly visible in Fig. 8, are listed in Table 3. Data for the $e^3\Sigma^- - X^1\Sigma^+$ (1,0)

band had previously been reported by Simmons and Tilford [39] and, at higher accuracy and also up to $J = 22$, by Lefloch *et al.* [40]. On average the data are offset by 0.04 cm^{-1} with respect to present values, which is within the error margins claimed in Ref. [40]. Term values of the $e^3\Sigma^-$ ($v = 1$) level can also be obtained via measurement of lines in the $B^1\Sigma^+ - e^3\Sigma^-$ system, with observations of the (0,1) band [41] at accuracies in the range 0.001–0.02 cm^{-1} combined with the measurements of the $B^1\Sigma^+ - X^1\Sigma^+(0,0)$ band, accurate at 0.003 cm^{-1} [42]. In comparison with the present data set the overall offset on the term values is within 0.015 cm^{-1} , which is well within the quoted uncertainties.

Observed lines associated with the $d^3\Delta - X^1\Sigma^+$ system are listed in Table 4 for the (4,0) band, observed for rotational angular momenta of $J = 26 - 36$, and in Table 5 for the (5,0) band, with observation of $J = 0 - 17$. In an investigation by Herzberg *et al.* [43] rotational levels up to $J = 22$ were observed in both bands at low accuracy. The observations in the $d^3\Delta - X^1\Sigma^+(4,0)$ band were superseded by those

Table 4: Observed transition frequencies (in vacuum cm^{-1}) of the CO $d^3\Delta - X^1\Sigma^+(4,0)$ band obtained with the hot cell. The estimated uncertainty (1σ) is 0.02 cm^{-1} except for weak or blended lines.

J''	F_1			F_2			F_3
	R(J)	Q(J)	P(J)	R(J)	Q(J)	P(J)	Q(J)
26	64610.70	64544.08					
27		64507.33					
28			64400.24				
29				64579.94	64504.55		
30				64532.81	64465.22	64389.87	
31				64495.05	64414.40	64346.77	
32					64372.81	64292.14	64464.02
33				64510.13	64421.74		
34				64458.06	64380.33		
35					64324.46	64246.83	
36						64187.21	

Table 5: Observed transition frequencies (in vacuum cm^{-1}) of the CO $d^3\Delta - X^1\Sigma^+(5,0)$ band obtained with the hot cell. The estimated uncertainty (1σ) is 0.02 cm^{-1} except for weak or blended lines.

J''	F_1			F_2		
	R(J)	Q(J)	P(J)	R(J)	Q(J)	P(J)
0				66210.18		
1				66211.77		
2	66176.59			66212.17	66204.04	66198.61
3	66174.74			66211.19	66200.58	
4	66171.62		66149.75	66209.16	66195.87	66185.22
5			66140.16		66189.94	
6	66160.90	66143.98		66201.11	66182.70	66166.87
7			66116.88	66195.03	66174.17	66155.80
8				66187.68	66164.30	66143.38
9				66178.92	66153.03	66129.72
10		66095.82		66168.86	66140.42	66114.67
11			66053.23	66157.25	66126.61	66098.22
12				66144.58	66111.32	66080.43
13				66130.29	66094.65	66061.40
14				66114.67	66076.58	66040.93
15				66097.74	66057.17	66019.02
16					66036.44	65995.79
17					66014.27	65971.17

Table 3: Observed transition frequencies (in vacuum cm^{-1}) of the CO $e^3\Sigma^- - X^1\Sigma^+(1,0)$ band obtained with the hot cell. The estimated uncertainty (1σ) is 0.02 cm^{-1} except for weak or blended lines.

J''	F_1		F_2		F_3	
	$^Q\text{R}(J)$	$^O\text{P}(J)$	$^Q\text{Q}(J)$	$^S\text{R}(J)$	$^Q\text{P}(J)$	
2			64798.89			
3	64794.01		64794.98			
4			64789.71	64788.84		
5		64759.37	64783.15	64782.45		
6	64811.33		64775.34	64774.92	64746.55	
7	64807.10	64764.30	64766.22	64766.60	64732.49	
8	64801.53		64755.89	64758.41	64717.25	
9		64741.55	64744.31	64794.65	64701.25	
10	64726.00		64731.92	64786.42	64685.41	
11		64656.88	64718.79	64776.94	64713.88	
12	64696.16	64637.39	64705.72		64698.09	
13	64679.05	64615.71	64674.65	64754.31	64680.93	
14		64592.43	64658.00		64662.50	
15		64567.68	64639.20	64728.76	64642.97	
16			64618.52	64703.94	64622.54	
17			64596.30	64688.01	64602.10	
18			64572.61		64569.64	
19			64547.41		64545.95	
20					64520.00	
21			64493.11		64492.39	
22					64463.22	

Table 6: Observed transition frequencies (in vacuum cm^{-1}) of other CO electronic-vibrational bands obtained with the hot cell. The estimated uncertainty (1σ) is 0.02 cm^{-1} except for weak or blended lines.

$D^1\Delta - X^1\Sigma^+(1,0)$		$a'^3\Sigma^+ - X^1\Sigma^+(9,0)$	
$^P\text{P}(26)$	65916.49	$^P\text{Q}1(39)$	64245.88
$^P\text{P}(27)$	65875.99	$d^3\Delta - X^1\Sigma^+(5,1)$	
$^Q\text{Q}(24)$	66050.52	$^R\text{Q}31(3)$	64057.44
$^Q\text{Q}(25)$	66016.10	$^R\text{Q}31(4)$	64052.92
$^Q\text{Q}(26)$	65979.36	$I^1\Sigma^- - X^1\Sigma^+(2,0)$	
$^R\text{R}(25)$	66078.85	$^Q\text{Q}(34)$	65837.46
$^R\text{R}(27)$	66011.16	$^Q\text{Q}(35)$	65785.95

Table 7: The updated molecular constants for the $A^1\Pi$ ($v=0$) and ($v=1$) states of $^{12}\text{C}^{16}\text{O}$ and the perturber states $d^3\Delta$ ($v=4$) and $D^1\Delta$ ($v=1$) following from the perturbation analysis. In cases where an uncertainty is specified in () parentheses the value was determined from the fit; in cases where this is not specified a value was taken from literature. For the $A^1\Pi$ states, the T_v and B parameters are fixed to the previous work[7], because these parameters are predominantly determined by the low- J transition frequencies. All values in vacuum cm^{-1} .

$A^1\Pi(v=0)$		$A^1\Pi(v=1)$	
T_v	64746.762	T_v	66228.801
B	1.604069	B	1.58126
$q (\times 10^5)$	1.4 (4)	$q (\times 10^5)$	-2.5 (4)
$D (\times 10^6)$	7.352 (5)	$D (\times 10^6)$	7.438 (4)
$H (\times 10^{12})$	-8 (2)	$H (\times 10^{12})$	-15 (1)
$d^3\Delta(v=4)$		$D^1\Delta(v=1)$	
T_v	65101.90 (3)	T_v	66462.11 (9)
B	1.23381 (8)	B	1.2373 (3)
A	-16.52 (1)		
λ	1.15 (3)		
$\gamma (\times 10^3)$	-8.54		
$D (\times 10^6)$	6.80 (6)	$D (\times 10^6)$	8.8 (4)
$H (\times 10^{12})$	-0.8	$H (\times 10^{12})$	-0.3
$A_D (\times 10^4)$	-1		
η_0	-21.72 (1)	ξ_0	0.040
η_1		ξ_1	0.077 (1)

of Lefloch *et al.* [40] at higher accuracy. Comparison with the latter and the present data set yields agreement within 0.04 cm^{-1} , hence within the quoted error margin of 0.06 cm^{-1} in Ref. [40].

The $d^3\Delta - X^1\Sigma^+(5,0)$ band had been investigated by VUV laser-induced fluorescence measurements [44]. Accurate data on this band were also reported from classical spectroscopic studies by Lefloch [45]; for this set the agreement with the present data is within 0.02 cm^{-1} . The $d^3\Delta$ ($v = 5$) levels were also observed in emission in the $B^1\Sigma^+ - d^3\Delta(0,5)$ band [41]. In the present study the F_1 and F_2 fine structure components in the $d^3\Delta$ state were observed, while in the study of Choe *et al.* [41] the F_3 components were seen as a result of different intensity borrowing. In addition two lines in the $d^3\Delta - X^1\Sigma^+(5,1)$ band were observed and listed in Table 6.

Additional lines observed were assigned to the $D^1\Delta - X^1\Sigma^+(1,0)$ band, the $I^1\Sigma^- - X^1\Sigma^+(2,0)$ band, and the $a^3\Sigma^+ - X^1\Sigma^+(9,0)$ band, and listed in Table 6. Some of these transitions probing perturber states were observed previously by Lefloch *et al.* [40, 45], although not all, and at a lower accuracy of 0.06 cm^{-1} . Herzberg *et al.* observed states up to $J = 22$ in the $I^1\Sigma^- - X^1\Sigma^+(2,0)$ band [46]. Despite the fact that information on the intermediate J -levels is missing, an unambiguous assignment of the transitions originating in $J = 34 - 35$ could nevertheless be made based on the perturbation patterns. The same holds for the newly observed lines in the $D^1\Delta - X^1\Sigma^+(1,0)$ band, for which rotational lines up to $J = 17$ were observed in the past [47], and for which new lines originating from $J = 24 - 26$ are found.

A reiteration of a previous deperturbation analysis for the $A^1\Pi$ ($v = 0$) and ($v = 1$) states [7] is performed including the additional data points for high- J levels. A comprehensive fit was performed based on the diagonalisation of a series of matrices containing J -dependent deperturbed energy levels and interaction energies of multiple states. The entire set of experimental $A^1\Pi - X^1\Sigma^+(0,0)$ and $(1,0)$ lines were reproduced and all lines exciting perturber states. The form of these perturbation matrices is kept the same as that defined in Table 6 of Ref. [7], keeping the

same labels for the parameters. For the $A^1\Pi$ states, the T_v and B parameters are fixed to the previous work[7], because these parameters are predominantly determined by the low- J transition frequencies. Most of the molecular constants resulting from this procedure did not undergo a significant change except for the values pertaining to the states $D^1\Delta(v = 1)$ and $d^3\Delta(v = 4)$. These values are listed in Table 7. The main difference for the $d^3\Delta$ state entails the inclusion of a quartic centrifugal distortion D and a spin-spin coupling constant, λ . Values for the $D^1\Delta$ state were previously kept constant but are now optimized in the present fit.

The rotational temperature $T_{rot} = 927 \pm 20 \text{ K}$ is determined by fitting the transition intensities of transitions with different J -quantum numbers, assuming a Boltzmann distribution of ground state populations. This fitting considers perturber states borrowing intensity from the $A^1\Pi - X^1\Sigma^+$ transitions. The vibrational temperature, $T_{vib} \sim 845 \text{ K}$, is calculated by comparing the intensities of the strong $A^1\Pi - X^1\Sigma^+(1,0)$ band and the weak $(1,1)$ hot band. For this analysis pressure saturation effects must be considered that prevent a direct comparison of intensities of these two vibrational bands with very different cross sections. Instead, spectra recorded at different column densities are used, also involving a comparison with the $A^1\Pi - X^1\Sigma^+(0,0)$ band of intermediate strength. Further, Franck-Condon factors of the $(1,0)$ and $(1,1)$ vibrational transitions must be considered, which are taken from Ref. [48]. The kinetic temperature, associated with Doppler broadening, is determined at $T_{kin} \sim 900 \text{ K}$.

5. Conclusion

Vacuum-ultraviolet photoabsorption spectra of N_2 and CO were recorded at 930 K using a heated free-flowing gas cell and the Fourier-transform spectrometer end station of the DESIRS beamline at the SOLEIL synchrotron. This novel setup allowed for the measurement of rotational transitions with angular-momentum quantum numbers, J' , as high as 51 and also from the first excited ground state vibrational level, which is well beyond the limit of room-temperature experiments. The high-resolution spec-

trometer permitted quantification of rotationally-resolved transition energies, f -values, and predissociation broadening for many vibrational bands.

In CO, we deduce new high- J' level energies for the upper states of the $A^1\Pi - X^1\Sigma^+(v', v'' = 0)$ bands with $v' = 0$ and 1, as well as observe new forbidden transitions to levels of the $e^3\Sigma^-$, $d^3\Delta$, $D^1\Delta$ and $a'^3\Sigma^+$ states. The forbidden transitions appear due to intensity-borrowing from the $A - X$ bands and the new data permitted an improved estimate of molecular parameters describing the forbidden levels and their perturbing interactions.

We measure new level energies, f -values, and predissociation linewidths of the N_2 bands $b^1\Pi_u - X^1\Sigma_u^+(v', v'' = 0)$ for $v' = 0, 1, 2$, and 10. These verify the high- J' predictions of a CSE model which was constructed with respect to room-temperature experimental data. This validates the use of photodissociation cross sections calculated from this model in atmospheric or astrophysical applications at high temperatures. No forbidden levels are observed for the case of N_2 . Instead, the J' -dependent widths of $b(v')$ provide new indirect information on an interacting dissociative manifold of $^3\Pi$ levels. The analysis of perturbed $b(10)$ level energies and linewidths permitted the characterisation of its level crossing with a $^3\Pi_u$ level of mixed electronic character.

There is some indication that for both target molecules the rotational and vibrational temperatures are not identical, 930 and 800–830 K, respectively. The incomplete equilibration of vibrational and rotational excitation will not affect our conclusions regarding the perturbation of high J' levels but introduces uncertainty into any determination of hot-band absolute f -values.

The present measurements of high-temperature cross sections and line lists have a direct application to the study of astrophysical environments and planetary atmospheres. It also provides detailed extra information on the underlying electronic states of the molecules and their non-Born-Oppenheimer interactions. This information, when incorporated with the larger experimental record, is necessary for constraining predictive models of the photoabsorbing and dissociating excited states; and will allow for improvements to the N_2 CSE model, and similar theoretical

developments for the case of CO.

Acknowledgements

This work is financially supported by the Dutch Astrochemistry Network of the Netherlands Foundation for Scientific Research (NWO). We wish to thank JF Gil, technician on the DESIRS beam line for the mechanical conception of the hot cell. We are grateful to the general and technical staff of SOLEIL for providing beam time under project n°20120653.

References

- [1] L. Nahon, N. de Oliveira, G. A. Garcia, J. F. Gil, B. Pilette, O. Marcouille, B. Lagarde, F. Polack, *J. of Synchrotron Rad.* **19**, 508-520 (2012).
- [2] N. de Oliveira, D. Joyeux, D. Phalippou, J.-C. Rodier, F. Polack, M. Vervloet, and L. Nahon, *Rev. Scient. Instr.* **80**, 043101 (2009).
- [3] N. de Oliveira, M. Roudjane, D. Joyeux, D. Phalippou, J.-C. Rodier, and L. Nahon, *Nat. Phot.* **5**, 149-153 (2011).
- [4] G. D. Dickenson, T. I. Ivanov, M. Roudjane, N. de Oliveira, D. Joyeux, L. Nahon, L. Tchang-Brillet, M. Glass-Maujean, I. Haar, A. Ehresmann, and W. Ubachs, *J. Chem. Phys.* **133**, 144317 (2010).
- [5] T. I. Ivanov, G. D. Dickenson, M. Roudjane, N. de Oliveira, D. Joyeux, L. Nahon, W.-L. Tchang-Brillet, and W. Ubachs, *Mol. Phys.* **108**, 771-786 (2010).
- [6] A. N. Heays, G. D. Dickenson, E. J. Salumbides, N. de Oliveira, D. Joyeux, L. Nahon, B. R. Lewis, and W. Ubachs, *J. Chem. Phys.* **135**, 244301 (2011).
- [7] M. L. Niu, E. J. Salumbides, D. Zhao, N. de Oliveira, D. Joyeux, L. Nahon, R. W. Field, W. Ubachs, *Mol. Phys.* **111**, 2163-2174 (2013).

- [8] L. E. Archer, G. Stark, P. L. Smith, J. R. Lyons, N. de Oliveira, L. Nahon, D. Joyeux, D. Blackie, J. Quant. Spectr. Rad. Transfer **177**, 88-92 (2013).
- [9] G. Stark, A. N. Heays, J. R. Lyons, P. L. Smith, M. Eidelsberg, S. R. Federman, J. L. Lemaire, L. Gavilan, N. de Oliveira, D. Joyeux, L. Nahon, *Astroph. J.* **788**, 67 (2014).
- [10] M. Eidelsberg, J. L. Lemaire, S. R. Federman, G. Stark, A. N. Heays, Y. Sheffer, L. Gavilan, J. H. Fillion, F. Rostas, J. R. Lyons, P. L. Smith, N. de Oliveira, D. Joyeux, M. Roudjane, L. Nahon, *Astron. Astrophys.* **543**, A69 (2012).
- [11] L. Gavilan, J. L. Lemaire, M. Eidelsberg, S. R. Federman, G. Stark, A. N. Heays, J.-H. Fillion, J. R. Lyons, and N. de Oliveira, *J. Phys. Chem. A* **117**, 9664-9652 (2013).
- [12] S. R. Federman, M. Fritts, S. Cheng, K. M. Menningen, D. C. Knauth, and K. Fulk, *Astroph. J. Suppl. Ser.* **134**, 133138 (2001).
- [13] A. de Lange, G. D. Dickenson, E. J. Salumbides, W. Ubachs, N. de Oliveira, D. Joyeux, L. Nahon, *J. Chem. Phys.* **136**, 234310 (2012).
- [14] A. N. Heays, R. Visser, R. Gredel, W. Ubachs, B. R. Lewis, S. T. Gibson, E. F. van Dishoeck, *Astron. Astrophys.* **562**, A61 (2014).
- [15] J. Bagdonaite, E. J. Salumbides, S. P. Preval, M. A. Barstow, J. D. Barrow, M. T. Murphy, and W. Ubachs, *Phys. Rev. Lett.* **113**, 123002 (2014).
- [16] F. Brandi, I. Velchev, W. Hogervorst, and W. Ubachs, *Phys. Rev. A* **64**, 032505 (2001).
- [17] E. B. Saloman, *J. Phys. Chem. Ref. Data* **33**, 765-922 (2004).
- [18] E. J. Salumbides, M. L. Niu, J. Bagdonaite, N. de Oliveira, D. Joyeux, L. Nahon, and W. Ubachs, *Phys. Rev. A* **86**, 022510 (2012).
- [19] W. Ubachs, L. Tashiro, and R. N. Zare, *Chem. Phys.* **130**, 1-13 (1989).
- [20] P. F. Levelt and W. Ubachs, *Chem. Phys.* **163**, 263-275 (1992).
- [21] J. P. Sprengers, W. Ubachs, A. Johansson, A. L'Huillier, C.-G. Wahlström, R. Lang, B. R. Lewis, and S. T. Gibson, *J. Chem. Phys.* **120**, 8973-8978 (2004).
- [22] J. P. Sprengers, W. Ubachs, and K. G. H. Baldwin, *J. Chem. Phys.* **122**, 144301 (2005).
- [23] G. Stark, K. P. Huber, K. Yoshino, P. L. Smith, and K. Ito, *J. Chem. Phys.* **123**, 214303 (2005).
- [24] G. Stark, B. R. Lewis, A. N. Heays, K. Yoshino, P. L. Smith, and K. Ito, *J. Chem. Phys.* **128**, 114302 (2008).
- [25] W. Ubachs, R. Lang, I. Velchev, W.-Ü. L. Tchang-Brillet, A. Johansson, Z. S. Li, V. Lokhnygin, and C.-G. Wahlström, *J. Chem. Phys.* **270**, 215-225 (2001).
- [26] B. R. Lewis, S. T. Gibson, W. Zhang, H. Lefebvre-Brion, and J. M. Robbe, *J. Chem. Phys.* **122**, 144302 (2005).
- [27] V. E. Haverd, B. R. Lewis, S. T. Gibson, and G. Stark, *J. Chem. Phys.* **123**, 214304 (2005).
- [28] B. R. Lewis, A. N. Heays, S. T. Gibson, H. Lefebvre-Brion, and R. Lefebvre, *J. Chem. Phys.* **129**, 164306 (2008).
- [29] A. N. Heays, J. M. Ajello, A. Aguilar, B. R. Lewis, and S. T. Gibson, *Astroph. J. Suppl. Ser.* **211**, 28 (2014).
- [30] P. Lavvas, M. Galand, R. V. Yelle, A. N. Heays, B. R. Lewis, G. R. Lewis, and A. J. Coates, *Icarus* **213**, 233-251 (2011).
- [31] X. Li, A. N. Heays, R. Visser, W. Ubachs, B. R. Lewis, S. T. Gibson, and E. F. van Dishoeck, *Astron. Astrophys.* **555**, A14 (2013).
- [32] A. N. Heays, R. Visser, R. Gredel, W. Ubachs, B. R. Lewis, S. T. Gibson, and E. F. van Dishoeck, *Astron. Astrophys.* **562**, A61 (2014).

- [33] X. Liu, D. E. Shemansky, C. P. Malone, P. V. Johnson, J. M. Ajello, I. Kanik, A. N. Heays, B. R. Lewis, S. T. Gibson, and G. Stark, *J. Geophys. Res.* **113**, A02304 (2008).
- [34] S. Edwards, J. Y. Roncin, F. Launay, and F. Rostas, *J. Mol. Spectrosc.* **162**, 257-267 (1993).
- [35] B. R. Lewis, S. T. Gibson, J. P. Sprengers, W. Ubachs, A. Johansson, and C.-G. Wahlström, *J. Chem. Phys.* **123**, 236101 (2005).
- [36] C. Y. Robert Wu, D. L. Judge, M.-H. Tsai, Y.-C. Lin, T.-S. Yih, J.-I. Lo, H.-S. Fung, Y.-Y. Lee, B. R. Lewis, A. N. Heays, and S. T. Gibson, *J. Chem. Phys.* **136**, 044301 (2012).
- [37] B. R. Lewis, K. G. H. Baldwin, J. P. Sprengers, W. Ubachs, G. Stark, and K. Yoshino, *J. Chem. Phys.* **129**, 164305 (2008).
- [38] A. B. van der Kamp, P. C. Cosby, and W. J. van der Zande, *Chem. Phys.* **184**, 319-333 (1994).
- [39] J. D. Simmons and S. G. Tilford, *J. Res. Nat. Bur. of Standards*, **75A**, 455-467 (1971).
- [40] A. C. Lefloch, F. Launay, J. Rostas, R. W. Field, C. M. Brown, K. Yoshino, *J. Mol. Spectr.* **121**, 337-379 (1987).
- [41] J.-I. Choe, D.-K. Lee, A. C. Lefloch, and S. G. Kukolich, *J. Mol. Spectrosc.* **136**, 173-184 (1989).
- [42] M. Drabbels, J. Heinze, J. J. ter Meulen, and W. L. Meerts, *J. Chem. Phys.* **99**, 5701-5711 (1993).
- [43] G. Herzberg, T. J. Hugo, S. G. Tilford, and J. D. Simmons, *Can. J. Phys.* **48**, 3004-3015 (1970).
- [44] A. Du Plessis, E. G. Rohwer, and C. M. Steenkamp, *J. Mol. Spectrosc.* **243**, 124-133 (2007).
- [45] A. C. Lefloch, Ph.D. thesis, Univ. Paris-Sud (1989).
- [46] G. Herzberg, J. D. Simmons, A. M. Bass, and S. G. Tilford, *Can. J. Phys.* **44**, 3039-3041 (1966).
- [47] J. D. Simmons and S. G. Tilford, *J. Chem. Phys.* **45**, 2965-2968 (1966).
- [48] L. W. Beegle, J. M. Ajello, G. K. James, D. Dziczek, and M. Alvarez, *Astron. Astrophys.* **347**, 375-390 (1999).